# Development of novel Chitosan / Guar Gum inks for extrusion-based 3D Bioprinting: Process, Printability and Properties

Franck Cleymand, Aurelia Poerio, Aziz Mamanov, Kamil Elkhoury, Lynda Ikhelf, Jean-Philippe Jehl, Cyril J.F. Kahn, Marc Poncot, Elmira Arab-Tehrany, João F. Mano

# Development of novel Chitosan / Guar Gum inks for extrusion-based 3D Bioprinting: Process, Printability and Properties.

*F. Cleymand* [a,d*], *A. Mamanov* [a], *A. Poerio* [a], *K. Elkhoury* [b], *J.P. Jehl*[a], *C.J.F. Kahn*[b], *M. Ponçot*[a], *E. Arab-Tehrany* [b], *João F. Mano*[a,c]

[a] Université de Lorraine, Institut Jean Lamour, UMR CNRS 7198, 2 allée André Guinier, Campus Artem, BP 50840, F-54011 Nancy Cedex, France

[b] Université de Lorraine, Laboratoire Ingénierie des Biomolécules, TSA 40602, Vandoeuvre-lès-Nancy, F-54518, France.

[c] University of Aveiro, CICECO—Aveiro Institute of Materials, Department of Chemistry 3810-193 Aveiro, Portugal

[d] Mines Nancy, Campus ARTEM, 92 rue du sergent Blandan, BP 14234, 54042 Nancy Cedex

*Corresponding author: franck.cleymand@univ-lorraine.fr

## Keywords

Chitosan; Guar gum; Ink; 3D Bioprinting; Hydrogel.

## Abstract

The major limitation of 3D bioprinting is the availability of inks. In order to develop new ink formulations, both their rheological behavior to obtain the best printability and the target bio-printed objects conformities must be studied. In this paper, the preparation and the characterization of novel ink formulations based on two natural polysaccharides, chitosan (CH) and guar gum (GG), are presented for the first time, in our knowledge. Five ink formulations containing different proportions of CH and GG were prepared and characterized in terms of rheological properties and solvent evaporation. Their printability was assessed (by varying nozzle diameter, pressure and speed) using an extrusion-based bio-printing process performed directly in air at 37°C. Results showed that the incorporation of GG improved both the printability of the pure chitosan inks by increasing the viscosity of the solution and the shape fidelity by accelerating the solvent evaporation. We showed that the ink containing 15% of GG

had the best printability. This formulation was therefore used for the preparation of membranes that were characterized by infrared spectroscopy (FTIR) and X-Ray Diffraction (XRD) before and after gelation as well as for their mechanical properties (Young modulus, strength and strain at break). In this case, optimal process printing parameters were determined to be 27 G micronozzle, printing pressure below 2 bars and robot head speed between 20 and 25 mm/s. This novel ink formulation is a guideline for developing 2D scaffolds (such as auto-supported membranes) or 3D scaffolds for biomedical applications.

## 1. Introduction

Due to the persistent problem of organ shortage, new artificial methods have been developed in order to find alternative solutions to transplantation [1-3]. 3D bioprinting has emerged as a promising method to fabricate complex devices to regenerate or replace tissues and organs that could be processed using natural polymers [4]. Among the different technologies, extrusion-based 3D bioprinting is the most commonly used in the field of health care applications [5]. Two approaches can be used for the extrusion-based bioprinting: the older one that consist on the deposition of the bioink on a flat surface in air and a more recent one where the bioink is extruded into a suspension bath that prevent the material to collapse [6]. However, the first one offers lower cost processability and less complexity. Despite the great progresses that have already been made, extrusion-based 3D bioprinting is still at its early stages and there are still lots of improvements to be made concerning the bioink availability [7]. One of the biggest limitations of this technology is the development of bioinks that, in form of hydrogels, present adequate mechanical properties to ensure a good printability and shape fidelity post-printing [8] without compromising the cell viability [9]. Either synthetic or natural materials can be used to prepare bioinks, which generally show opposite characteristics. In fact, while synthetic materials present strong mechanical properties simplifying the printing process and shape fidelity of the printed constructs, the natural ones present low immunogenicity and higher biocompatibility, biodegradability, and bioactivity properties [10]. Among the different biomaterials, natural polymers have been gaining increased interest because of their ability to mimic the extracellular matrix (ECM), offering the adequate environment to support cell proliferation and viability [11-12]. Chitosan (CH) is the second most abundant biopolymer found in nature, obtained by the deacetylation of chitin that can be extracted from the exoskeleton of crustaceans [13]. CH has

several biological properties such as biocompatibility, biodegradability and bioactivity [14]. Furthermore, it has antimicrobial properties that make it suitable for tissue engineering applications [15]. However, because of the lack of strong mechanical properties and slow rate of gelation (that is important for the shape fidelity after printing) CH alone is not suitable for proper and easy printing [16]. Therefore other macromolecules are often necessary. CH was already mixed with synthetic materials like PLA [17] or hydroxyapatite [18], natural ones like gelatin [19] and catechol [20] to produce bioinks for 3D bioprinting. We hypothesize that the combination of CH with other natural polysaccharides, such as Guar Gum (GG), could create a new component of bioink suitable for the extrusion-based 3D bioprinting. GG is a water-soluble microbial polysaccharide, composed of a linear chain of 1,4-linked mannose residues to which galactose residues are 1,6-linked at every second mannose [21]. GG has been used as a stiffener agent and appropriate for many pharmaceutical and food applications [22]. For example, CH-GG hydrogels have been used to create transdermal patch for the delivery of paracetamol and showed low cytotoxicity and antimicrobial activity in vitro [23]. Furthermore, thanks to its ability of forming gels in water, GG is used to increase the viscosity of solutions representing a great candidate as a component of bioinks [24]. The aim of this study was to develop CH/GG ink formulation using different proportions of the two polymers and optimizing the printing parameters in order to achieve a good printability. Ink formulations were then characterized in terms of viscosity, solvent evaporation, dimensional stability and shape fidelity before and after gelation by neutralization. Membranes created using the formulation that showed the best printability were object of further studies such as infrared spectroscopy, X-ray diffraction and mechanical properties (Young's modulus, strength and strain at break), before and after gelation. We will show that the inclusion of GG improved the mechanical properties and consequently the printability of pure CH as well as its dimensional stability leading to a better post bio-printing behavior.

## 2. Materials and methods

### 2.1. Materials

Chitosan (CH) 90% deacetylated, 15 mPa.s viscosity was purchased from Heppe Medical Chitosan GmbH, Germany. Guar Gum (GG), Citric Acid monohydrate (CA) and Acetic Acid

(AA) > 99.8% were obtained from Sigma-Aldrich. Ethanol absolute came from Carlo Erba. NaOH was obtained from VWR.

### 2.2. Inks formulations

Ink formulations were adapted from the previous methods used to elaborate films [25, 26, 27]. Pure CH solution and pure GG solution were mixed in different proportions to create the ink formulations (labelled C100, C95, C85, C75 and C65) described in **Table 1**, by pouring GG into CH [26]. Pure CH solutions were prepared by dissolving 10% w/v CH in a 40% (v/v) acetic acid solution in Deionized Water (DW) at 25°C. Then, 3% (w/v) CA followed by 10% w/v CH was slowly added to the solution, and mechanical mixed overnight. Then, the solution was centrifuged at 3,000 rpm for 10 min (Heraeus Multifuge X) and kept to rest for 2 hours at 25°C to remove undissolved particles and air bubbles. To prepare pure GG solution, 1.5% w/v GG was first mixed with absolute ethanol (0.5 mL of ethanol for 100 mg of GG) to avoid GG aggregation in the solution, then poured into DW at 80°C and mixed for 5 mins [28]. Then, the solution was kept resting for 2 hours at 25°C to let the viscosity increase with the decrease of the temperature. Finally, different proportions of pure CH and pure GG solutions were mixed under agitation at 70°C for 30 mins and kept for 1 h at 25°C. Then, each ink formulation was centrifuged at 3,000 rpm for 10 mins to eliminate all remaining air bubbles, before being poured into a syringe. Syringes were sealed, covered with aluminum foil and stored in a fridge at 4°C until usage. The density of each ink formulation, calculated by measuring the mass of 1 mL of ink (in triplicate), is presented in **Table 1**.

**Table 1.** Composition of the different ink formulations with respective densities CH: chitosan, GG: guar gum

| | **C100** | **C95** | **C85** | **C75** | **C65** |
|---|---|---|---|---|---|
| **CH (%)** | 100 | 95 | 85 | 75 | 65 |
| **GG (%)** | 0 | 5 | 15 | 25 | 35 |
| **Density ($g.cm^{-1}$)** | 1.186 | 1.183 | 1.182 | 1.175 | 1.158 |

### 2.3. 3D Bioprinting processes

In this study, a 4th generation 3D-Bioplotter from EnvisionTEC controlled with Visual Machine software, was used to perform all the printing processes. This bioprinter was equipped with a temperature-controlled platform (-10 to 80°C) fixed at 15°C and a low temperature dispensing head (0 to 70°C) fixed at 37°C to print all the ink formulations under uniform conditions. The ink was inserted in a 30 mL syringe equipped with a blue end cap to prevent ink flow before use. Then a white SmoothFlow™ piston was inserted and the syringe was fixed to a high-pressure blue adapter (Nordson EFD). Ink formulations were extruded through SmoothFlow™ tapered micronozzle (22 G: 410 µm, 25 G: 250 µm, 27 G: 200 µm, Nordson EFD) under applied pressure controlled by an air-powered dispensing system.

### 2.4. Rheological characterization of the ink formulations.

Shear viscosities and shear thinning property of the ink formulations were determined using a rotational rheometer Malvern Kinexus™ (Malvern Instruments Ltd., Malvern, UK) fitted with a cone plate geometry (4° and 40 mm diameter) at shear rates range of 0.01-1000 $s^{-1}$ at 37°C. The edge of the cone-plate was covered with mineral oil to prevent solvent evaporation.

### 2.5. Solvent content and evaporation rate

The variation in the solvent content and the evaporation rates of all CH/GG ink formulations were investigated. Individual lines (length: 78 mm), called filaments in the following, were extruded through a 25 G micronozzle at a robot head speed of 5 $mm.s^{-1}$ and at a pressure of 1.2 bars. The weight loss, representative of a decrease in the solvent content, was measured using a high precision balance (OHAUS Adventurer Pro) for 3-4 hours and after drying the filaments for 2 days at 25°C. The evaporation rate was then calculated by dividing the weight variation by the initial weight of printed filaments.

### 2.6. Determination of optimal bio-printing parameters

The flow rate of the five ink compositions under different pressures and nozzles were determined. In order to study the effect of the printing parameters, filaments (length: 78 mm) were printed on a Petri dish using the 5 ink formulations (presented in **Table 1**) under different pressures, robot head speed and extruded from different nozzles (22, 25 and 27 G). The images

of the printed filaments were captured with an optical binocular Stevui S11. Three random parts of each filament (from three samples per each group) were measured and the best printability was obtained for the ink formulation that presented the lowest filament diameter (d), the lowest variation between the theoretical surface (Sth) and the real surface (Sr), the lowest sprawl and the highest dimensional stability. The ink formulation C65 was used to select the appropriate nozzle size. In order to do this, the ink was extruded using the 25 and 27 G nozzles at a fixed speed of 5 $mm.s^{-1}$ under a pressure range of 0.9-2.5 bars. Then, the formulation C85, printed using a 27 G micronozzle, was used to evaluate the influence of different robot head speed (15, 20, 25 and 30 $mm.s^{-1}$) and extrusion pressure (from 1.5 to 4 bars). Lastly, the influence of the ink composition on the diameter of printed filaments was assessed by printing the 5 different ink formulations with a 25 G micronozzle, a robot head speed of 25 $mm.s^{-1}$ and a pressure range between 0.9 and 2.5 bars. Eventually, the ink formulation C85 was selected as an optimal composition for extrusion based-printing and was the object of further studies after printing.

### 2.7. Gelation by Neutralization

After printing C85 rectangular membranes (width = 20 mm, length = 80 mm) were printed using a 25 G micronozzle, under a pressure of 1.5 bar and a robot head speed of 10 $mm.s^{-1}$. Gelation was obtained by immersing membranes in a 1M sodium hydroxide (NaOH) solution for 18h. After this time, membranes were washed with DW to remove excess of NaOH until neutral pH was achieved and dried in an oven at 50°C for 4h. For this and the following studies, neutralised membranes in a wet state will be named NW, while neutralized membranes in a dry state will be named ND. Similarly, as-printed membranes in a wet state will be named APW, while as-printed membranes in a dry state will be named APD.

### 2.8. Dimensional stability analysis

To determine the effect of gelation on dimensional stability, neutralized C85-based membranes (length=79 mm, width=39.5 mm) were compared to as-printed ones. The size variation (length and width) was measured using Panasis 2.3.3 Software while they were drying at 25°C, at 0, 2, 4, 18 and 24 hours. All measurements were performed in triplicate.

### 2.9. X-ray diffraction (XRD)

XRD spectra of as-printed in a dried state (APD) and neutralized in a dried state (ND) C85-based membranes were recorded using a D8 Advance diffractometer. Data were collected in the 2θ scan angle range of 5-55° with a scan rate of 0.6°/min (2s/step) and 0.02°/step. The machine was set at 40 kV and 40 mA at RT. All samples were dried in an oven during 4h at 50°C before use.

### 2.10. Fourier transform infrared spectroscopy (FTIR)

FTIR spectra were obtained with a Thermo Scientific Nicolet machine on as-printed in a dried state (APD) and neutralized in dried state (ND) C85-based membranes. Analysis were performed with 64 scans and a 4000-400 $cm^{-1}$ spectral range (4 $cm^{-1}$ resolution).

### 2.11. Mechanical properties of the printed rectangular membranes

Young's modulus and tensile properties (strength and strain at break) of the as-printed (APW and APD) and neutralized (NW and ND) rectangular membranes (width = 20 mm, length = 80 mm) prepared using C85 as ink were investigated using an electromechanical machine with a 100N load cell and following the standard of ASTM D3822/D3822M. To achieve a wet state, samples were immersed in DW during 24h before use. The tensile tests were done at least 5 times per each condition.

## 3. Results and discussion

### 3.1. Rheological properties

The size of the nozzle and the ink composition are two important parameters that determine the flow rate, described as the quantity of ink filament leaving the nozzle tip per unit time. The effect of different nozzle diameters and pressures on the C65 ink formulation and the effect of the composition of the inks extruded using the same nozzle diameter were examined. **Figure 1A** shows the volumetric flow rate of C65 ink under different extrusion pressures and three different micronozzles (22 G: 410 µm, 25 G: 250 µm, 27 G: 200 µm). Without any surprise, the flow rate increased when the nozzle diameter increased at a given pressure. **Figure 1B** shows the evolution of flow rate for all ink formulations, fixing the micronozzle (25 G), under different pressure. All the curves had a general tendency represented by a monotonous linear increasing as applied pressure increase. Using C100 as reference curve, two ink presented curves located below it (C85 and C95) while two inks presented curves located above it (C65 and C75). This

phenomenon could be explained by the thixotropic behavior of inks. As mentioned in [25], it is worth noting that, on the one hand, the amino groups of CH are protonated to $NH_3+$ in the acetic acid solution and on the other hand, the ordered structures of GG are destroyed with the solubilization process, resulting in intermolecular hydrogen bonding between $NH_3+$ of the CH backbone and $OH^-$ of the GG. From pure CH to 15% of GG content the formation of hydrogen bonding increased the viscosity. When the concentration of GG increase from 15% to 35%, a reduction in viscosities of inks formultations containing GG was observed.

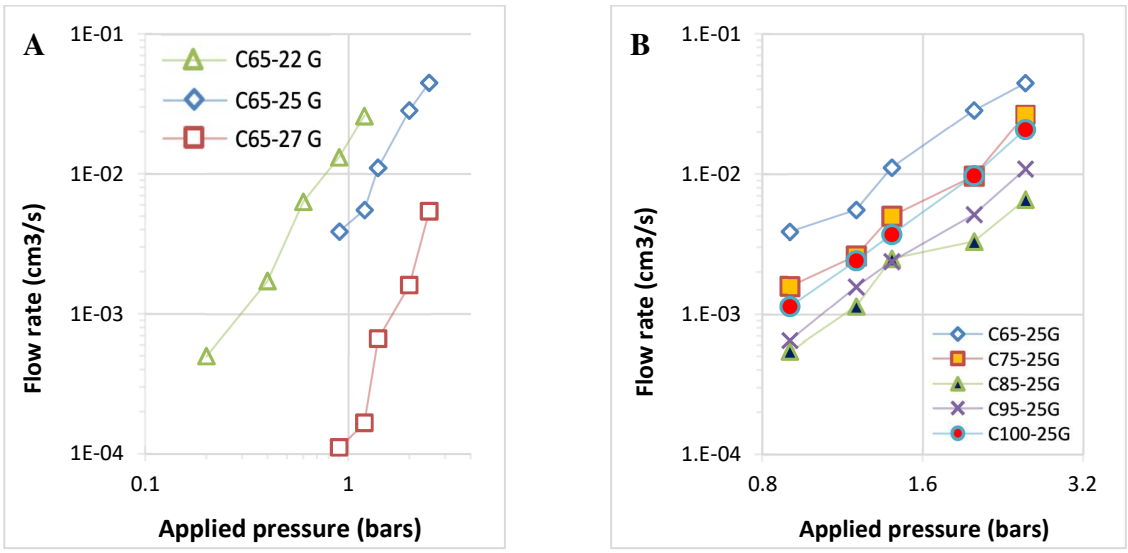


**Figure 1:** Volumetric flow rate as a function of applied pressure. (A) C65 ink deposited using three micronozzles (22, 25, 27 G) and (B) five different inks (C65 to C100) extruded with a 25 G micronozzle.

Ink viscosity is one of the most important parameters for a successful bioprinting. Inks should preferentially present a shear thinning behavior, in order to allow an easy continued and regular flow through the nozzle when pressure is applied during the extrusion. **Figure 2** shows the viscosity of the different ink formulations. All ink formulations exhibited a shear thinning behavior and could be suitable for extrusion-based bioprinting because they decrease their viscosity under increasing pressure. Results show that the inclusion of GG on pure CH solution increase its viscosity, although this increase in not directly dependent on the added quantity. In

fact, C75 presented the highest viscosity at share rate of $0.1s^{-1}$, followed by C65, C95, C85 and lastly C100. The higher viscosity of C95 compared to C85 could probably be explained by the fact that the initial increase in GG's concentration resulted in intermolecular hydrogen bonding between $NH_3$+ of the CH backbone and $OH^-$ of the GG, but further addition of GG led to decrease the puncture force as mentionned in [14], and could be attributed to the aggregation of the GG double helices. These observations can be linked to the amphiphilic nature of the two polysaccharides used. Both C95 and C85 results show that a reduced shear rate is necessary in order to achieve the loss of viscosity: 0.8 Pa.s is obtained at 63 $s^{-1}$ for C95 and 125.9 $s^{-1}$ for C85, against 158 $s^{-1}$ for C100. This property is interesting because it allows a potential reduction in applied pressure during bio-printing, that could be advantageous if the inclusion of cells during the bioprinting is considered. Furthermore, the use of low pressure and thus the creation of thinner filaments could improve the shape fidelity after printing. For instance, viscosity of C85 and C95 dropped from 100 Pa.s at a steady state of 0.3 Pa.s at a shear rate of 200 $s^{-1}$. All this type of ink became unstable above 100 $s^{-1}$ shear rates. Results concerning C75 and C65 were unstable, probably due to their lack of homogeneity and phase separation of the ink over time.

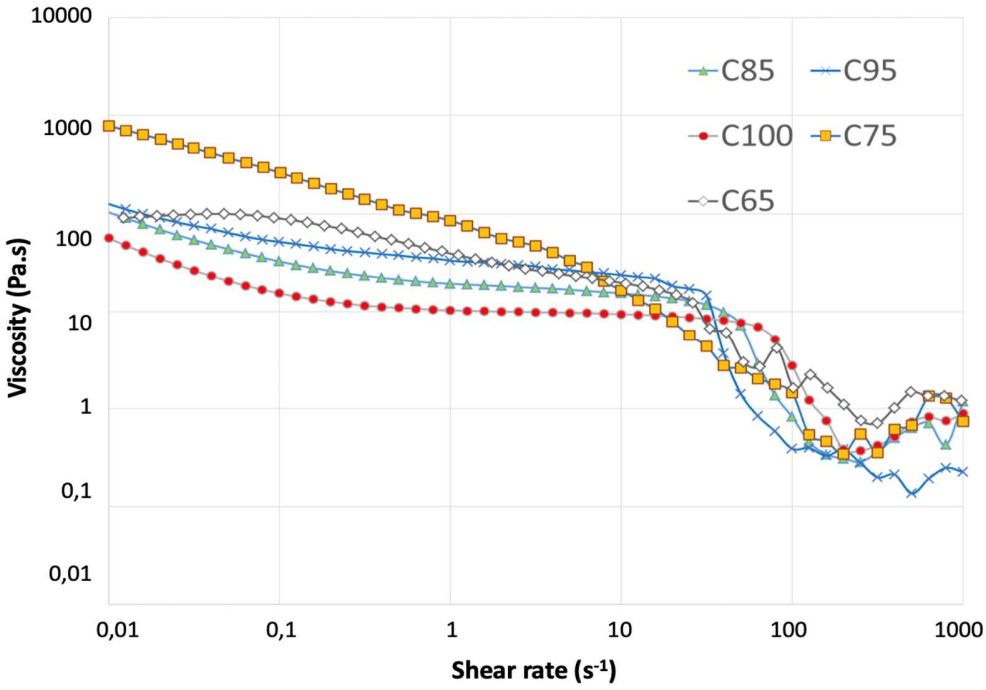


**Figure 2.** Viscosity (Pa.s) as a function of shear rate ($s^{-1}$) for C65, C75, C85, C95 and C100 ink formulations.

### 3.2. Solvent evaporation rate

Solvent evaporation rate is an important parameter that can affect the dimensional stability and printability of bioinks [27]. In fact, a faster solvent evaporation rate leads to a faster solidification of the printed structure. Consequently, the possibility to build complexes 3D structures without collapsing phenomena increases.

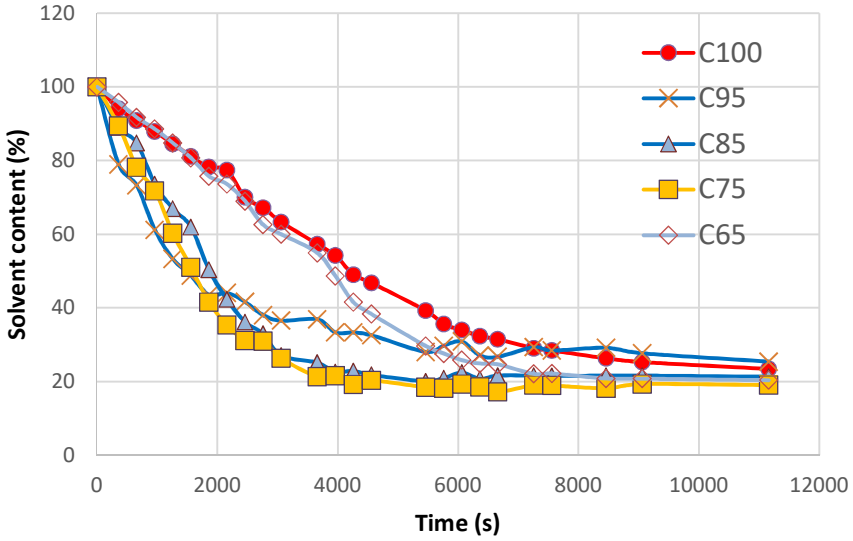


**Figure 3.** Time dependency of the solvent content inside the filaments printed with all inks, obtained through weight measurements at 25°C.

**Figure 3** shows the evolution of the solvent content (%) as a function of time for all ink formulations. All samples exhibited a large tendency to stabilize around a solvent content of 25%, proving that GG did not influence drastically the final solvent content. This amount was similar to the results presented by Wu *et al.* [27] for a 8% CH solution prepared in acetic acid while the same solution prepared in an acidic mixture of 40% AA, 20% Lactic Acid (LA) and 3% CA lead to a final solvent content of 40% due to its lower vapor pressure (0.0813 mmHg at 25°C for LA and 15.7 mmHg for CA). These results showed that acetic acid is more prone to evaporation into air than lactic acid. But the acid mixture used contained non-volatile CA, which results in residual solvent in the filaments and can therefore minimize the drying-induced shrinkage. The evolution of the solvent content of C75, C85 and C95 follow similar trends with a

fast initial decrease while C100 and C65 show a more linear dependence. Furthermore, there is no significant difference in the curve of C85 and C75 in comparison to C65. This can be explained by the fact that the presence of GG reduces the oxygen barrier property of the bio-printed structure which led to a better exchange with the atmosphere [14]. Moreover, according to Kester and Fennema [29], a higher concentration of GG (as in C65) increases the oxygen permeability, meaning that a part of the evaporated solvent is rapidly replaced by oxygen. The ink evaporation rates, showed in **Table 2**, were obtained from the linear regression of the solvent content loss curves in its linear part. The evaporation rate was lower for the pure CH ink and for the formulation containing the highest % of GG (C65) at values of 0.0016 $s^{-1}$ and 0.0130 $s^{-1}$, respectively. However, the ink formulations with decreasing content of GG presented an increase of the evaporation rate.

**Table 2.** Evaporation rate of the ink formulations obtained from the linear regression of the solvent content loss curves during the first 50 mins for C95, C85 and C75 inks and the first 90 mins for C100 and C65 inks in the initial stage.

| **Ink** | **C100** | **C95** | **C85** | **C75** | **C65** |
|---|---|---|---|---|---|
| **Evaporation rate (%.$s^{-1}$)** | 0.0116 | 0.0333 | 0.0254 | 0.0273 | 0.0130 |

In comparison with Wu *et al.* results, an acidic mixture of AA and LA could be more appropriate to increase solvent retention and to induce lower shrinkage [27]. However, to be used as bio-ink, it would be preferable to have a faster solvent evaporation rate to avoid negative consequences after the incorporation of cells. Because of the faster evaporation rate, the ink formulations containing a percentage of GG comprised between 5 and 25 resulted more appropriate in order to obtain greater shape fidelity after printing.

### 3.3. Influence of speed, pressure, nozzle diameter and ink composition on printability

The study of the printability of filaments is an effective way to define the potential of inks for 3D bioprinting. Despite the absence of a standard definition of the term printability there are some basic requirements for an ink to be considered printable. First of all, the extrudability that represent the capability to achieve extrusion and second of all the shape fidelity of the final

construct that can be evaluated on single layers by measuring the size of printed filaments [9]. **Figure 4A** shows the diameter of C65 printed filaments at a robot head speed of 5 mm/s under different pressure using two different gauges (25 and 27 G). Using the 27 G it was possible to print filaments with smaller diameters for any applied pressure, due to the smaller nozzle diameter and higher shear rate in it. The difference in filament diameter was from 2.84 (0.9 bars) to 4.36 times bigger (2 bars) when using the 25 G. This phenomenon can be attributed to a high pressure in the micro-nozzle, inducing an increase in the shear rate and, *a fortiori,* an alignment of the ink macromolecules. Then, after extrusion, the macromolecules tend to reorganize and take on a less dense configuration. Moreover, while the pressures rise, the amount of ink that flows out is much higher as well. Therefore, 27 G allows a higher precision during printing. The influence of different robot head speed (15, 20, 25 and 30 mm/s) and extrusion pressure (from 1.5 to 4 bar) was examined by printing C85 ink with a 27 G micronozzle (see **Figure 4B**). Results show that when a 200 µm nozzle (27 G) was used and the pressure was higher than 2.1 bars, the diameter of the filaments was higher than 300 µm. In addition, the high-pressure relaxation effect indicated that it would be more interesting to work with pressures below 2.1 bars. Under this pressure, the values of the printed diameters split in two distinct regions: the first one for speeds of 15 and 20 mm/s with filament ranging [300 µm - 400 µm], and the second one for speeds 25 and 30 mm/s with D ranging [200 µm-300 µm]. To study the influence of the ink composition, the nozzle (25 G) and the speed (25 mm/s) were fixed and the different ink formulations were extruded under different pressures (from 0.9 to 2.5 bar). **Figure 4C** shows a representative 3D map of the diameter of printed filaments. As expected, the diameter of the filaments was smaller for lower pressures, while, when the pressure increases, the ink flow was higher and consequently, the diameter. For a given pressure, we obtained better results for the inks referenced C75, C85 and C95. Indeed, an almost symmetric tendency around C85 was observed, which means that C85 was the best candidate. The lowest possible diameter for C75 and C95 using a pressure of 0.9 bar was between 1 and 1.5 mm, whereas using the same pressure but C85 as ink, the diameter decreased at values comprised between 0.5 and 1 mm. As a consequence, keeping in mind the wish to have filaments diameters the closest possible to the diameter of the nozzle used (D ≅ DG), the optimal parameters for 3D bio-printing (speed 25 mm/s and pressure below 2 bars) were given by the green region of the 3D map in **Figure 4C.**

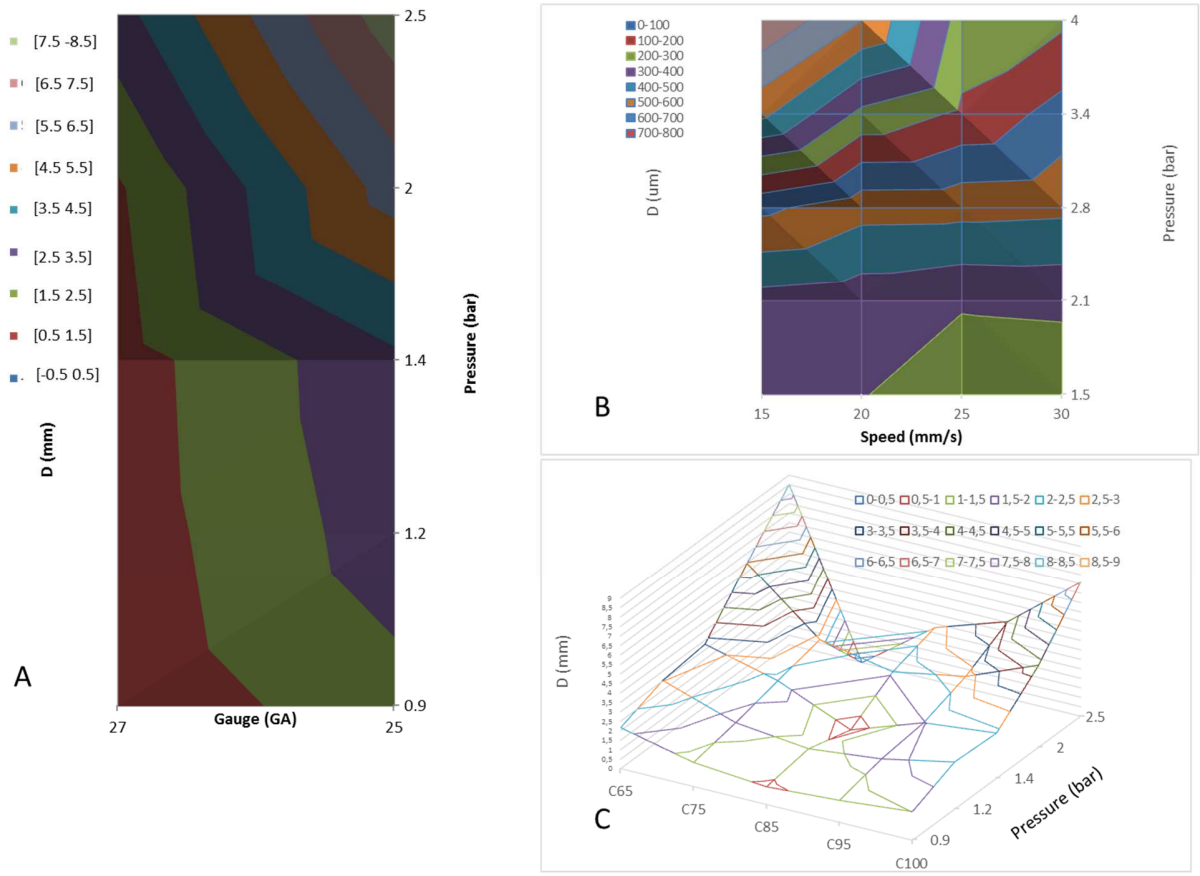


**Figures 4.** (A) Process map illustrating the diameter of C65 ink obtained filaments (colors) with respect to the applied pressure during extrusion and micronozzle used. (B) Process map illustrating the diameter of C85 obtained filaments (colors) with respect to the applied pressure and robot head speed used. (C) 3D map of the of all the ink formulation diameter obtained with respect to applied pressure and ink used. Zones where the diameter is the lowest are privileged.

The optical images in **Figures 5** highlight the ink's sprawling for all formulations of filaments printed at a pressure of 2 bars, a speed of 5 $mm.s^{-1}$ and a 25 G nozzle. The filaments printed using C65 and C100 ink exhibited sprawling along the edges and gave non-linear filaments, while C75 and C95 resulted in less sprawling effect and a slight roughness was still present. Instead, the filament printed using C85 as ink had straight and smooth edges. The filaments printed with C85 ink had had the best stability right after printing.

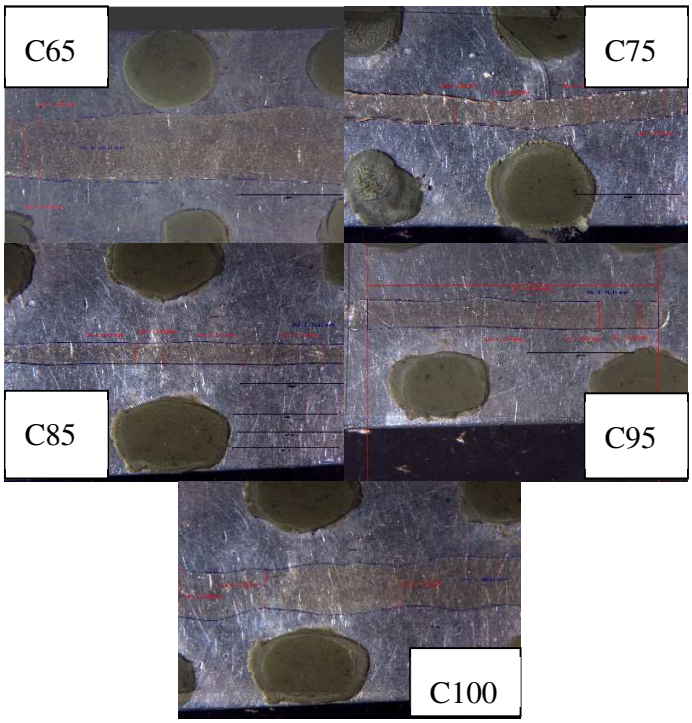


**Figures 5.** Optical images taken by a binocular showing the visual sprawling of all inks at 2 bars, 5 mm/s and 25 G micronozzle.

An alternative method for the study of the sprawling effect is presented in **Figure 6**. This method is based on the measure of the difference between the apparent and the theoretical surface, calculated by multiplying the average diameter of the filament by the length of the filament (hypothesis of the zero-default ink). The apparent surface was measured using Panasis software. When this value is close to 0% it means that the apparent surface of printed filament fit the theoretical surface it should have. C65 and C100 had values between 5% and 10% of difference between the apparent and theoretical surface, confirming the sprawling effect. C75 and C95 showed also a difference between 5 and 10% for low pressure and high pressure respectively. Instead, C85 had values between 0 and 5% for any applied pressure, representing the best ink formulation in terms of sprawling effect. These results suggested also that the inclusion of GG between 5% and 25%, allowed a good printability with reference to the diameter of the filaments and the sprawling effect (Figure 4C, 5 and 6).

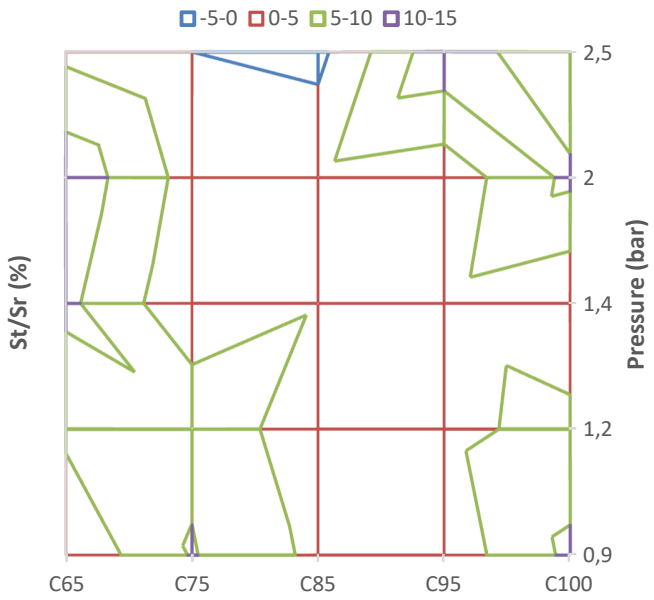


**Figure 6.** Mapping of the difference in percent between theorical printed surface and real surface in function of pressure and ink used. Value equal to 0 means that there are absolute no sprawl.

### 3.4. Dimensional stability of as-printed and post-neutralized membranes

Membranes printed with C85 ink formulation were used to study the dimensional stability. Right after printing, membranes were stored at 25°C to allow solvent evaporation. The shrinkage of the printed membranes was evaluated by measuring their length (L) and width (W) after 0 (as-printed), 2, 18 and 24h. The same data were collected on membranes after neutralization with 1 M NaOH. Experiments were done in triplicate. Because of there were no variations in the width, only the length was measures. **Figure 7** shows the effect of this shrinkage over time on filaments as printed and after neutralization.

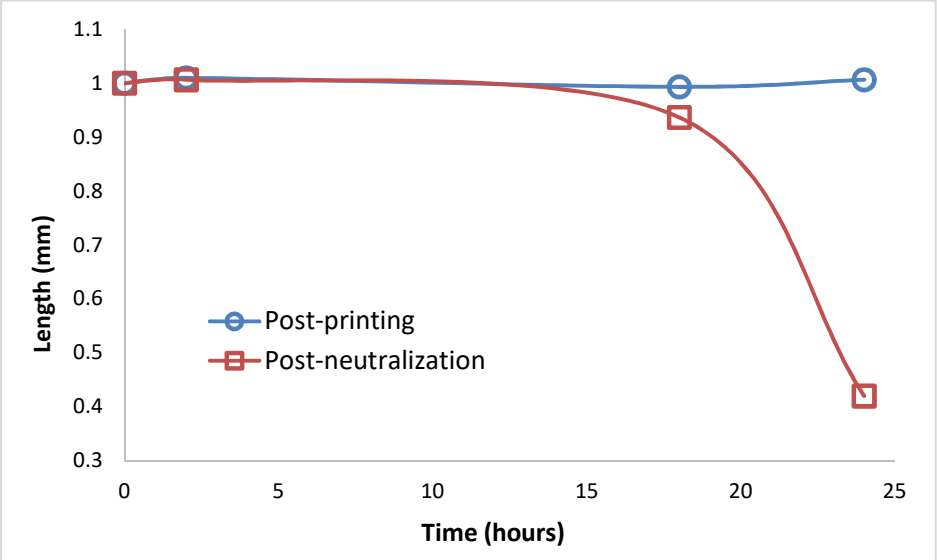


**Figure 7.** Length variation over time of C85 printed membranes post-printing and post-neutralization.

The length of membranes printed with C85 ink did not change after 24 hours indicating that it could be possible to print entire scaffolds requiring long-printing time without shrinkage problem. No shrinkage was detected after 24h of solvent evaporation. The neutralization step with 1M NaOH was used to remove the residual acid and obtain hydrogels. **Figures 8** shows the morphological variation of membranes during the different processing steps. **Figure 8A** corresponds to as-printed or directly post-printing membrane (initial state). The printed membranes directly after printing were completely smooth. After 24h at 25°C, the dried membranes (**Figure 8B**) presented a wrinkled surface and air bubbles that got stuck. After 24 hours of neutralization with 1M NaOH, the samples (**Figure 8C**) had a visible size reduction and started to shrink (2.5 to 10% reduction) due to the evaporation of water. During the neutralization, $NH_3^+$ groups are deprotonated, the ionic repulsion between the chains of the two polysaccharides decrease and the release of water increase thus the packing of the macromolecular chains and gel shrinkage were promoted [19]. A shrinkage of 55-62% of the initial length of neutralized membranes was observed after 24 h drying (**Figure 8D**). Membranes were completely deformed after drying 24h in air.

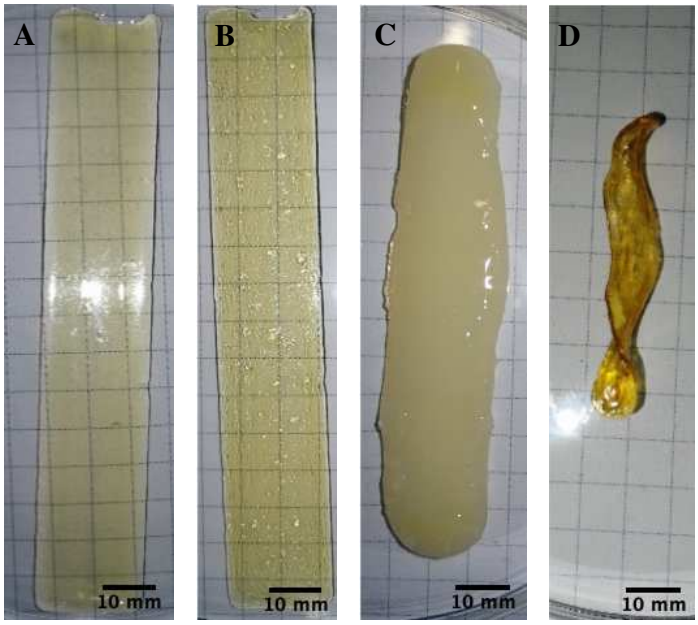


**Figures 8.** Morphological variation of rectangular membranes (20 mm x 80 mm) using C85 ink formulation during different steps: (A) as-printed or directly post-printing (initial state), (B) after 24h drying at 25°C, (C) post-neutralization and (D) after 24h drying after neutralization.

In order to study the shrinkage post process, comparison between as printed, after neutralization and after the washing step, were proceeded. Membranes (length=79 mm, width=39.5 mm) were prepared using C85 ink. The shrinkage was quantified measuring the relative size reduction over the process. **Table 3** shows the dimensional variation of membranes after neutralization and after washing with DW. Washing step allow to remove excess of NaOH solution and to obtain membranes at neutral pH. This step could be interesting if the introduction of cells is wished after printing.

**Table 3**: Dimensional variation over the process of C85 printed sample with 79 mm length and a square section of 39.5 mm width. Measures were taken right after the steps without any modification.

| | As-Printed | After neutralization | After Washing |
|---|---|---|---|
| **Length (mm)** | 1 | 0.96 | 0.95 |
| **Width (mm)** | 1 | 1.02 | 0.98 |
| **Width (mm)** | 1 | 0.95 | 0.91 |

The length and width of the samples were reduced from 5% and 3% to 10% respectively. This may be explained by the fact that the printed sample absorbed a great amount of water during neutralization and washing steps. During these steps, all samples maintained their shapes.

### 3.5. XRD characterization

XRD patterns of as-printed in a dried state (APD) and neutralized in a dried state (ND) C85-based membranes are presented in **Figure 9**. ADP membranes presented a sharp peak at 2θ = 12° (from 10° to 14°) and a broad peak from 16° to 26° with a maximum at 20°. Wu *et al.* [27] showed that pure CH printed filaments did not present the peak at 12° while it appears after neutralization with NaOH. The presence of this peak in CH/GG membranes could mean that the introduction of GG allows a higher crystallinity leading to greater mechanical properties [15]. However, the large peak around 20°, associated with amorphous phase of CH [20], implies that some solvent remained after drying. GG macromolecules can expand the spacing between chitosan chains, interaction between the amino groups of chitosan and the carboxyl group in citric acid. Same observations have been done when using lactic acid [21]. After neutralizing, the same peak is seen at 2θ = 12° but the peak at 20° became much thinner and lost its intensity. This could be due to the loss in acidity and to an increase of crystalline degree.

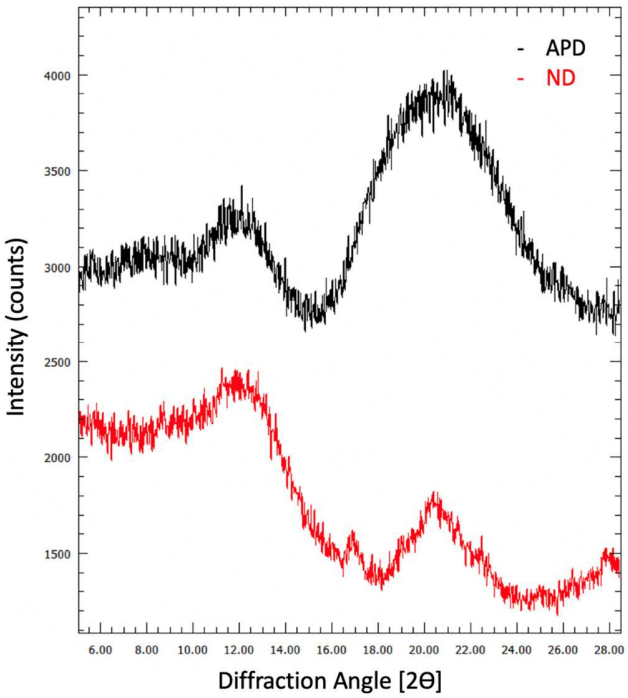

**Figure 9:** XRD spectrum of as-printed in a dried state (APD) and neutralized in a dried state (ND) C85-based membranes

### 3.6. FTIR analysis

FTIR spectra presented in **Figure 10** highlight the bonding and functional groups present in CH/GG as-printed in a dried state (APD) and neutralized in a dried state (ND) C85-based membranes. In general, both states showed the same spectrum with no significant difference in peaks position. In both states, a broad peak is observed between 3100-3600 $cm^{-1}$ with a maximum at 3550 $cm^{-1}$, linked to stretching vibration of -OH groups [26, 30]. In addition, the peak at 2890 $cm^{-1}$ is characteristic of C-H vibrations from $CH_2$ groups. A tiny residual peak due to ring stretching of GG at 1700 $cm^{-1}$ has been also determined. Amide I groups represented at 1530 $cm^{-1}$ from CH, and at 1350 $cm^{-1}$ one sharp peak representing C-H bending. Then an intense peak of all C-C groups at 1200 $cm^{-1}$. Finally, at 1070 $cm^{-1}$ and 980 $cm^{-1}$ there were ether C-O stretching vibration and C-OH stretching [23, 26, 30]. There was no evidence of linkage between GG and CH that would form a durable polymer. Adding a cross-linker would solve this problem as mentioned before [23]. Indeed, chitosan forms $NH_3^+$ when exposed to acidic environment, offering opportunities for anionic groups to establish electrostatic interactions.

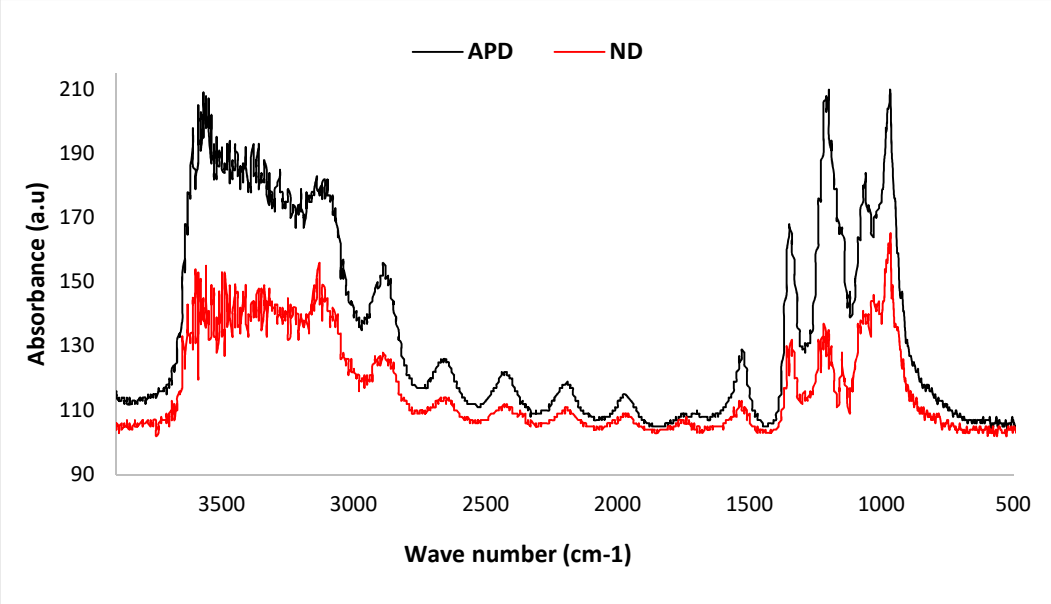

**Figure 10.** FTIR spectra of as-printed in a dried state (APD, black) and neutralized in a dried state (ND, red) C85-based membranes- ADP was dried in an oven after printing, ND was neutralized after printing before being dried in an oven.

### 3.7. Mechanical characterization

Young's modulus and tensile properties of as-printed membranes at a wet (APW) and dry (APD) state and neutralized membranes at a dry (ND) state were investigated. Due to their fragility, it was not possible to perform the mechanical tests on the neutralized membranes in a wet (NW) state. All membranes were printed using C85 as ink and had a rectangular shape (length = 80 mm, width= 20 mm). Young modulus values of the mentioned membranes were 1MPa, 280 MPa and 1GPa for APW, APD and ND membranes, respectively. The values are determined at around 20%. As expected, ADP membranes stiffness was higher than APW. Drying increases the rigidity of the membrane and the neutralization step makes the membranes more flexible. This is consistent with regard to the different protocols used for these steps. APD membranes presented a stress at break of 35 MPa whereas the stress at break for APW and ND was only 0.3 MPa and 7 MPa respectively (**Figure 11**). This last value was similar to the neutralized wet membranes made of pure CH (6 MPa) presented by Wu *et al.* [27]. **Figure 11** also shows the strain at break. Dry printed samples showed a low strain, which is close to the pure CH. Chains flexibility was not influenced by the presence of GG. The wet bioprinted membranes deformed to 31% of its initial length. Finally, GG mainly increase the limit strength break by increasing the interaction between CC and GG. Nonetheless crosslinking will be still necessary in order to maintain a better stability at the wet state.

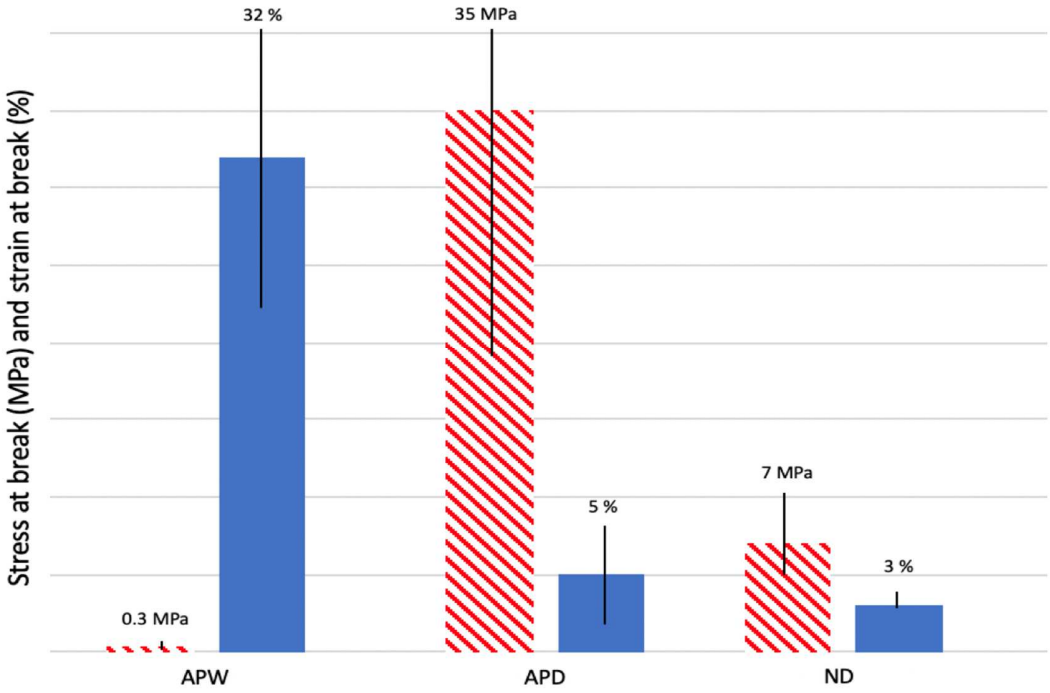


**Figure 11.** Tensile stress at break (red) and strain at break (blue) of as-printed membranes at a wet (APW) and dry (APD) state and neutralized membranes at a dry state (ND) C85-based.

## 4. Conclusions

We proposed for the first time the combination of chitosan (CH) and guar gum (GG) to develop new inks for extrusion-based 3D bioprinting. The influence of the ink composition, robot head speed, pressure and micronozzle size on the printability of 5 different ink formulations has been studied. Moreover, the inks characteristics such as rheological properties, solvent evaporation at different proportion of CH/GG gave important information on its printability and stability. 1D and 2D structures were successfully printed and analyzed. Improved mechanical properties and better dimensional stability were obtained with a 85% CH - 15% (w/v) GG ink. Further investigation must be made to examine the feasibility in the creation of 3D structures and to examine the biological properties such as biocompatibility and biodegradability. The ink presented in the study showed a good printability and the potential to be used in the field of the health care applications.

## Author contributions

The manuscript was written through the contributions of all authors. All authors have given approval to the final version of the manuscript.

## Conflict of interest

The authors declare that they have no known competing for financial interests or personal relationships that could have appeared to influence the work reported in this paper.

## Acknowledgment

This work was supported partly by the French PIA project “Lorraine Université d’Excellence”, reference ANR-15-IDEX-04-LUE, FC and JFM would also thanks “le cercle Gutenberg” and canceropôle Grand-Est for their financial support.

## References

[1] R. Langer, J. Vacanti, Tissue engineering, Science. 260 (1993) 920–926. https://doi.org/10.1126/science.8493529.

[2] A.S. Hoffman, Hydrogels for biomedical applications, Advanced Drug Delivery Reviews. 64 (2012) 18–23. https://doi.org/10.1016/j.addr.2012.09.010.

[3] K. Elkhoury, C. S. Russell, L. Sanchez-Gonzalez, A. Mostafavi, T. J. Williams, C. Kahn, N. A. Peppas, E. Arab-Tehrany, A. Tamayol, Soft-Nanoparticle Functionalization of Natural Hydrogels for Tissue Engineering Applications, Adv. Healthcare Mater., vol. 8, no. 18, p. 1900506, Sep. 2019, doi: 10.1002/adhm.201900506.

[4] H.-W. Kang, S. J. Lee, I. K. Ko, C. Kengla, J. J. Yoo, A. Atala, A 3D bioprinting system to produce human-scale tissue constructs with structural integrity, Nat Biotechnol, vol. 34, no. 3, pp. 312–319, Mar. 2016, doi: 10.1038/nbt.3413.

[5] S. V. Murphy, A. Atala, 3D bioprinting of tissues and organs, Nat Biotechnol, vol. 32, no. 8, pp. 773–785, Aug. 2014, doi: 10.1038/nbt.2958.

[6] A. McCormack, C. B. Highley, N. R. Leslie, F. P. W. Melchels, 3D Printing in Suspension Baths: Keeping the Promises of Bioprinting Afloat, Trends in Biotechnology, p. S0167779919303154, Jan. 2020, doi: 10.1016/j.tibtech.2019.12.020.

[7] A. Panwar, L. Tan, Current Status of Bioinks for Micro-Extrusion-Based 3D Bioprinting, Molecules, vol. 21, no. 6, p. 685, May 2016, doi: 10.3390/molecules21060685.

[8] Y. Jin, C. Liu, W. Chai, A. Compaan, Y. Huang, Self-Supporting Nanoclay as Internal Scaffold Material for Direct Printing of Soft Hydrogel Composite Structures in Air, ACS Appl. Mater. Interfaces, vol. 9, no. 20, pp. 17456–17465, May 2017, doi: 10.1021/acsami.7b03613.

[9] G. Gillispie, P. Prim, J. Copus, J. Fisher, A. G. Mikos, J J. Yoo, A. Atala, S. J. Lee, Assessment methodologies for extrusion-based bioink printability, Biofabrication, vol. 12, no. 2, p. 022003, Feb. 2020, doi: 10.1088/1758-5090/ab6f0d.

[10] J. Gopinathan, I. Noh, Recent trends in bioinks for 3D printing, Biomater Res, vol. 22, no. 1, p. 11, Dec. 2018, doi: 10.1186/s40824-018-0122-1.

[11] N. E. Fedorovich, J. Alblas, J. R. de Wijn, W. E. Hennink, A. J. Verbout, W. J. A. Dhert, Hydrogels as Extracellular Matrices for Skeletal Tissue Engineering: State-of-the-Art and Novel Application in Organ Printing, Tissue Engineering, vol. 13, no. 8, pp. 1905–1925, Aug. 2007, doi: 10.1089/ten.2006.0175.

[12] J. F. Mano, G. A. Silva, H. S. Azevedo, P. B. Malafaya, R. A. Sousa, S. S. Silva, L. F. Boesel, J. M. Oliveira, T. C. Santos, A. P. Marques, N. M. Neves and R. L. Reis, Natural origin biodegradable systems in tissue engineering and regenerative medicine: present status and some moving trends, J. R. Soc. Interface, vol. 4, no. 17, pp. 999–1030, Dec. 2007, doi: 10.1098/rsif.2007.0220.

[13] R. A. A. Muzzarelli, C. Muzzarelli, Chitosan Chemistry: Relevance to the Biomedical Sciences, in Polysaccharides I, vol. 186, T. Heinze, Ed. Berlin/Heidelberg: Springer-Verlag, 2005, pp. 151–209.

[14] M. S. Rao, S. R. Kanatt, S. P. Chawla, A. Sharma, Chitosan and guar gum composite films: Preparation, physical, mechanical and antimicrobial properties, Carbohydrate Polymers, vol. 82, no. 4, pp. 1243–1247, Nov. 2010, doi: 10.1016/j.carbpol.2010.06.058.

[15] M. Kong, X. G. Chen, K. Xing, H. J. Park, Antimicrobial properties of chitosan and mode of action: A state of the art review, International Journal of Food Microbiology, vol. 144, no. 1, pp. 51–63, Nov. 2010, doi: 10.1016/j.ijfoodmicro.2010.09.012.

[16] T. T. Demirtaş, G. Irmak, M. Gümüşderelioğlu, A bioprintable form of chitosan hydrogel for bone tissue engineering, Biofabrication, vol. 9, no. 3, p. 035003, Jul. 2017, doi: 10.1088/1758-5090/aa7b1d.

[17] C. R. Almeida, T. Serra, M. I. Oliveira, J. A. Planell, M. A. Barbosa, M. Navarro, Impact of 3-D printed PLA- and chitosan-based scaffolds on human monocyte/macrophage responses: Unraveling the effect of 3-D structures on inflammation, Acta Biomaterialia, vol. 10, no. 2, pp. 613–622, Feb. 2014, doi: 10.1016/j.actbio.2013.10.035.

[18] T.H. Ang, F.S.A. Sultana, D.W. Hutmacher, Y.S. Wong, J.Y.H. Fuh, X.M. Mo, H.T. Loh, E. Burdet, S.H. Teoh, Fabrication of 3D chitosan–hydroxyapatite scaffolds using a robotic dispensing system, Materials Science and Engineering: C, vol. 20, no. 1–2, pp. 35–42, May 2002, doi: 10.1016/S0928-4931(02)00010-3.

[19] W. L. Ng, W. Y. Yeong, M. W. Naing, Development of Polyelectrolyte Chitosan-gelatin Hydrogels for Skin Bioprinting, Procedia CIRP, vol. 49, pp. 105–112, 2016, doi: 10.1016/j.procir.2015.09.002.

[20] D. Lee, J. P. Park, M. Y. Koh, P. Kim, J. Lee, M. Shin, H. Lee, Chitosan-catechol: a writable bioink under serum culture media, Biomater. Sci., vol. 6, no. 5, pp. 1040–1047, 2018, doi: 10.1039/C8BM00174J.

[21] M. Srivastava, V. P. Kapoor, Seed Galactomannans: An Overview, C&B, vol. 2, no. 3, pp. 295–317, Mar. 2005, doi: 10.1002/cbdv.200590013.

[22] R. Mohammadinejad, A. Kumar, M. Ranjbar-Mohammadi, M. Ashrafizadeh, S. S. Han, G.Khang and Z. Roveimiab, Recent Advances in Natural Gum-Based Biomaterials for Tissue Engineering and Regenerative Medicine: A Review, Polymers, vol. 12, no. 1, p. 176, Jan. 2020, doi: 10.3390/polym12010176.

[23] A. J. Sami, M. Khalid, T.Jamil, S. Aftab, S. A. Mangat, A.R. Shakoori, S. Iqbal, Formulation of novel chitosan guargum based hydrogels for sustained drug release of paracetamol," International Journal of Biological Macromolecules, vol. 108, pp. 324–332, Mar. 2018, doi: 10.1016/j.ijbiomac.2017.12.008.

[24] D. Mudgil, S. Barak, B. S. Khatkar, Guar gum: processing, properties and food applications—A Review, J Food Sci Technol, vol. 51, no. 3, pp. 409–418, Mar. 2014, doi: 10.1007/s13197-011-0522-x.

[25] M. S. Rao, S. R. Kanatt, S. P. Chawla, A. Sharma, Chitosan and guar gum composite films: Preparation, physical, mechanical and antimicrobial properties, Carbohydrate Polymers, vol. 82, no. 4, pp. 1243–1247, Nov. 2010, doi: 10.1016/j.carbpol.2010.06.058.

[26] Y. Tang, X. Zhang, R. Zhao, D. Guo, J. Zhang, Preparation and properties of chitosan/guar gum/nanocrystalline cellulose nanocomposite films, Carbohydrate Polymers, vol. 197, pp. 128–136, Oct. 2018, doi: 10.1016/j.carbpol.2018.05.073.

[27] Q. Wu, D. Therriault, M.-C. Heuzey, Processing and Properties of Chitosan Inks for 3D Printing of Hydrogel Microstructures, ACS Biomater. Sci. Eng., vol. 4, no. 7, pp. 2643–2652, Jul. 2018, doi: 10.1021/acsbiomaterials.8b00415.

[28] N. Yagoub and A. O. Nur, "The influence of thermal treatment on physical properties of guar gum," Innovations in Pharmaceutical Sciences, vol. 2, no. 6, pp. 26–31, 2013.

[29] T. Wittaya, "Edible films and coatings: Characteristics and properties," International Food Research Journal, vol. 15, Jan. 2008.

[30] D.N. Iqbal, M. Tariq, S.M. Khan, N. Gull, S. Sagar Iqbal, A. Aziz, A. Nazir, M. Iqbal, Synthesis and characterization of chitosan and guar gum based ternary blends with polyvinyl alcohol, International Journal of Biological Macromolecules. 143 (2020) 546–554. https://doi.org/10.1016/j.ijbiomac.2019.12.043.